Analysis and Design of a Continuous-Wave Terahertz Photoconductive Photomixer Array Source

Daryoosh Saeedkia, *Member, IEEE*, Raafat R. Mansour, *Fellow, IEEE*, and Safieddin Safavi-Naeini, *Member, IEEE*

***Abstract*—An array of photoconductive photomixer/antenna elements as a continuous-wave terahertz source is proposed, and its radiation characteristic is studied. Employing photomixer/antenna elements in an array configuration increases available terahertz power, while each of the array elements consumes optical power less than its maximum sustainable power. A few microwatt terahertz power is achievable from a typical array structure. It is shown that the radiated beam can be steered by changing the angle between the two exciting laser beams.**

***Index Terms*—Continuous-wave terahertz sources, photomixers, terahertz antenna array, terahertz optoelectronics, ultrafast photoconductors.**

I. Introduction

TERAHERTZ technology is a fast growing field with applications in biology and medicine [1]–[4], imaging [5], [6], material spectroscopy and sensing [7]–[11], security [12]–[15], monitoring and spectroscopy in pharmaceutical industry [16], [17], and high-data-rate short-range communications [18]–[20].

Photomixers are promising continuous-wave terahertz sources as potentially compact, low-power-consuming, coherent, low-cost, and tunable sources [21]–[28]. A terahertz photomixer is a heterodyne scheme, in which output of two single-mode lasers or output modes of a dual-mode laser with their frequency difference falling in the terahertz range mix in a nonlinear medium, such as a photoconductor [27], [29] or a superconductor [30], and generate a signal, whose frequency is equal to the frequency difference of the two lasers or two modes of the dual-mode laser. The frequency of the generated terahertz signal can be tuned by tuning the central frequency of the lasers.

Narrow spectral bandwidth and frequency control of the photomixers make them suitable for the applications such as biological and material spectroscopy, medical imaging, and security, which need a tunable source over the terahertz spectrum. Photomixers also can be used as local oscillators in heterodyne receivers for radio astronomy and communication applications.

Recently, the authors have proposed an integrated photomixer/antenna structure as an efficient terahertz source [31], [32]. In a photomixer/antenna element, the generated signal inside the photomixing film radiates simultaneously by designing the film as an efficient radiator. Incorporating a photomixing medium as an antenna element not only eliminates any source-to-antenna coupling problem, but also distributes the optical power over a bigger area, and hence increases maximum applicable optical power to the device.

The maximum available terahertz power from a single element photoconductive photomixer source is limited by its maximum consumable optical power and maximum sustainable dc bias before device failure. A solution to this problem is using an array of photomixers. The simple optical excitation scheme in a photomixer/antenna element makes it suitable for an array structure. Since there is no need for a feeding network for an array of these elements, one can excite the entire array by two laser beams. One can increase the radiation power by increasing the number of array elements and using high power lasers. On the other hand, one can change the phase distribution of the photocurrent in array elements by changing the angle between the two laser beams and steer the radiated beam.

In this paper, we introduce an array of photoconductive photomixer/antenna elements as a high power tunable CW terahertz source. The radiation characteristics of the proposed structure is analyzed and the simulation results for a designed sample are presented.

II. Formulation

Fig. 1 shows an array of photoconductive photomixer/antenna elements. Photomixer elements are made of an ultra-fast photoconductor material, and are biased to a dc voltage by their bias electrodes. All the array elements are located above a grounded dielectric substrate. Two linearly polarized laser beams excite the entire structure. The corresponding electric field associated with each laser over the nmth element can be written as

$$E_{nm1(2)} = \left|E_{nm1(2)}\right| e^{j\left(\omega_{1(2)}t - \mathbf{k}_{nm1(2)}\cdot\mathbf{r}\right)} \tag{1}$$

where $n = -N,\ldots,N$, $m = -M,\ldots,M$, ω_1 and ω_2 are the angular frequencies of the lasers, $\mathbf{k}_{nm1}$ and $\mathbf{k}_{nm2}$ are the wave-vectors of the lasers over the nmth element, and $\mathbf{r}$ is the position vector over the same element. The lasers are assumed to be far enough from the surface of the photomixers so that the wave reaching each element can be assumed to be a local plane-wave. A uniform optical excitation can be achieved by coupling the laser beams to the array via an appropriate cylindrical lens.

Fig. 2 shows the array arrangement in $x-y$ plane. The wave-vectors $\mathbf{k}_{nm1}$ and $\mathbf{k}_{nm2}$ can be written as

$$\mathbf{k}_{nm1(2)} = k_{1(2)}\left[\cos\beta_{nm1(2)}\hat{x} + \cos\gamma_{nm1(2)}\hat{y} + \cos\theta_{nm1(2)}\hat{z}\right] \tag{2}$$

Manuscript received March 8, 2005; revised July 28, 2005. This work was supported by the NSERC/RIM Industrial Research Chair Program.

The authors are with the Electrical and Computer Engineering Department, University of Waterloo, Waterloo, ON N2L 3G1, Canada (e-mail: daryoosh@lenz.uwaterloo.ca).

Digital Object Identifier 10.1109/TAP.2005.859909

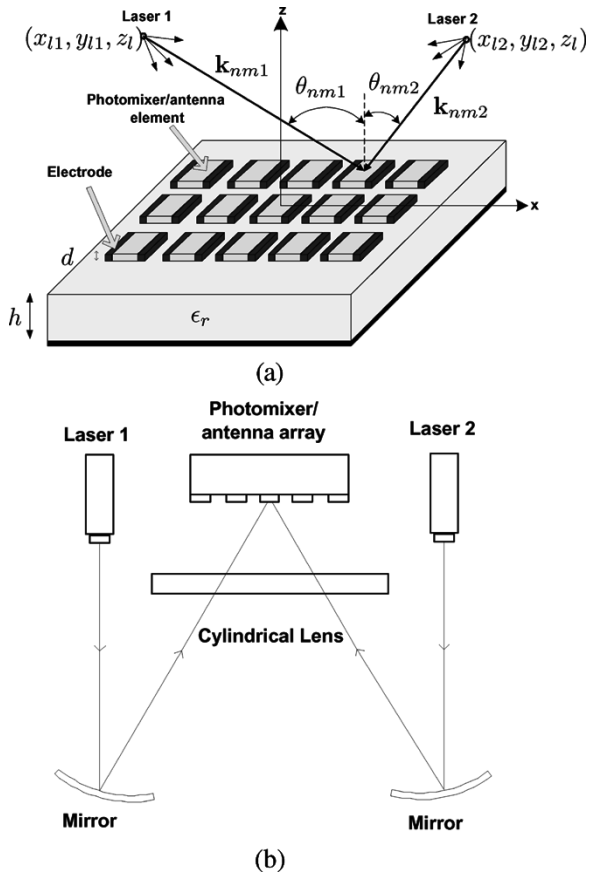

Fig. 1. (a) Photoconductive photomixer/antenna array configuration and (b) optical excitation scheme.

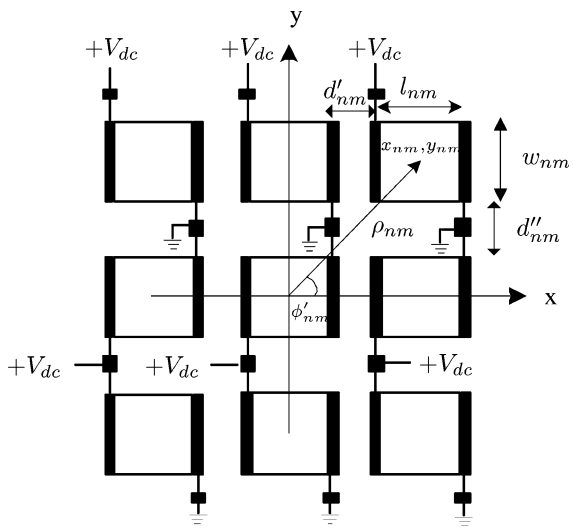

Fig. 2. Array arrangement in $(x-y)$ plane.

where k_1 and k_2 are the wave-numbers of the lasers in free space and

$$\cos\beta_{nm1(2)} = \frac{x_{nm}-x_{l1(2)}}{\left[\left(x_{nm}-x_{l1(2)}\right)^2+\left(y_{nm}-y_{l1(2)}\right)^2+z_l^2\right]^{\frac{1}{2}}} \quad (3)$$

$$\cos\gamma_{nm1(2)} = \frac{y_{nm}-y_{l1(2)}}{\left[\left(x_{nm}-x_{l1(2)}\right)^2+\left(y_{nm}-y_{l1(2)}\right)^2+z_l^2\right]^{\frac{1}{2}}} \quad (4)$$

$$\cos\theta_{nm1(2)} = \frac{-z_l}{\left[\left(x_{nm}-x_{l1(2)}\right)^2+\left(y_{nm}-y_{l1(2)}\right)^2+z_l^2\right]^{\frac{1}{2}}}. \quad (5)$$

The incident laser beams interfere inside the array elements and create a spatiotemporal optical intensity grating. Considering nonuniform absorption along the thickness of the photoconducting film, one can write the optical intensity inside the nmth element as

$$I_{nm}(\mathbf{r},t)=I_0T_{nm}(\theta_{nm1},\theta_{nm2})[1+\eta_{nm}\cos(\Omega t-\mathbf{K_{nm}}\cdot\mathbf{r})]e^{\alpha z} \quad (6)$$

where I_0 is the total optical intensity of the lasers, T_{nm} is the optical intensity transmission coefficient at photoconductor-air interface, α is the optical absorption coefficient, $0<\eta_{nm}\leq 1$ is the modulation index or grating contrast, $\Omega=\omega_1-\omega_2$ is the angular beat frequency, and $\mathbf{K_{nm}}=\mathbf{k}_{nm1}-\mathbf{k}_{nm2}$ is the grating vector.

The absorbed optical power inside the photoconductor material modulates the density of the electrons and holes in time and space by exciting electrons from valence band to conduction band. In the presence of a dc bias, the modulated electron and hole densities generate a current inside the photoconductor, which contains a beat frequency harmonic in its spectrum. It has been shown by the authors [29], [31] that the generated terahertz photocurrent inside a photomixer is a travelling-wave current, which can be written for the nmth element as

$$\tilde{J}^s_{nm}(x,y)=J^s_{nm}e^{-j[K_{nmx}x+K_{nmy}y+\phi_{nm}]} \quad (7)$$

where

$$K_{nmx}=k_1\cos\beta_{nm1}-k_2\cos\beta_{nm2} \quad (8)$$

$$K_{nmy}=k_1\cos\gamma_{nm1}-k_2\cos\gamma_{nm2} \quad (9)$$

$$J^s_{nm}=\left[(J^s_{nm1})^2+(J^s_{nm2})^2\right]^{\frac{1}{2}} \quad (10)$$

$$\phi_{nm}=\tan^{-1}\frac{J^s_{nm2}}{J^s_{nm1}}. \quad (11)$$

The expressions for J^s_{nm1} and J^s_{nm2} in terms of the physical parameters of the photomixer are given in Appendix I [29].

The current distribution in each element acts as a source of radiation. The electric current model [33] can be employed to obtain the far field radiation from each element as (see Fig. 2 for the definition of the parameters)

$$\begin{aligned}E^{nm}_{\theta(\phi)}(r,\theta,\phi)=&\,4E^{hex}_{\theta(\phi)}\tilde{J}_{snm}(x_{nm},y_{nm})\\&\times e^{jk_0\rho_{nm}\sin\theta\cos(\phi-\phi'_{nm})}\\&\times\frac{\sin\left[\frac{l_{nm}}{2}(k_0\sin\theta\cos\phi-K_{nmx})\right]}{K_{nmx}-k_0\sin\theta\cos\phi}\\&\times\frac{\sin\left[\frac{w_{nm}}{2}(k_0\sin\theta\sin\phi-K_{nmy})\right]}{k_0\sin\theta\sin\phi-K_{nmy}}\end{aligned} \quad (12)$$

where $E^{hex}_{\theta(\phi)}$ is the radiated electric field from an x-directed Hertzian electric dipole on a grounded dielectric substrate [33]

and k_0 is the free space wave-number. The superposition of all these radiated fields is the field produced by the array

$$E_{\theta(\phi)}(r,\theta,\phi)=\sum_{n=-N}^{N}\sum_{m=-M}^{M}E_{\theta(\phi)}^{nm}(r,\theta,\phi). \tag{13}$$

The total radiated power can be calculated using Poynting's vector theorem [34]

$$P_r=\frac{1}{2\eta_0}\int_0^{\frac{\pi}{2}}\int_0^{2\pi}\left[|E_\theta|^2+|E_\phi|^2\right]r^2\sin\theta\,d\phi d\theta \tag{14}$$

where η_0 is the free space impedance.

III. Analysis and Design

The primary goal is to have maximum radiation power, which from (12) for the nmth element occurs for

$$l_{nm}=\frac{\pi}{K_{nmx}}=\frac{\lambda_{nmx}}{2} \tag{15}$$

$$w_{nm}=\frac{\pi}{K_{nmy}}=\frac{\lambda_{nmy}}{2} \tag{16}$$

where λ_{nmx} and λ_{nmy} are the photocurrent spatial wavelengths along the x and y-axis, respectively. It can be seen from (8) that the x-component of the grating vector K_{nmx} is a relatively big number. From (15), the optimum values for the lengths of the array elements will be in the order of a few micrometers. On the other hand, the y-component of the grating vector K_{nmy} given by (9) is a small number and becomes zero for the array elements located on x-axis. Hence, from (16) one can conclude that the wider the array elements the higher the radiation power.

In (15) both l_{nm} and K_{nmx} are related to the position of the nmth element in $x-y$ plane. To find the optimum values of the lengths of the array elements from (15), one has to solve the following iterative equation for x_{nm}

$$\begin{aligned}x_{n(\pm m)}=&x_{n(\pm(m-1))}\pm\frac{1}{2}l_{n(\pm(m-1))}\\&\pm\frac{3\pi}{2}\left[\frac{\left(x_{n(\pm m)}-x_{l1}\right)k_1}{\left[\left(x_{n(\pm m)}-x_{l1}\right)^2+(y_{nm}-y_{l1})^2+z_l^2\right]^{\frac{1}{2}}}\right.\\&\left.-\frac{\left(x_{n(\pm m)}-x_{l2}\right)k_2}{\left[\left(x_{n(\pm m)}-x_{l2}\right)^2+(y_{nm}-y_{l2})^2+z_l^2\right]^{\frac{1}{2}}}\right]^{-1}\end{aligned} \tag{17}$$

where $m=1,\ldots,M$, $n=-N,\ldots,N$, $x_{n0}=0$, and

$$\begin{aligned}l_{n0}=\pi&\left[\frac{-x_{l1}}{[x_{l1}^2+(y_{n0}-y_{l1})^2+z_l^2]^{\frac{1}{2}}}k_1\right.\\&\left.+\frac{x_{l2}}{[x_{l2}^2+(y_{n0}-y_{l2})^2+z_l^2]^{\frac{1}{2}}}k_2\right]^{-1}\end{aligned} \tag{18}$$

TABLE I
LTG-GaAs Physical Parameters

Description	Notation	Value
Work temperature	T_0	300 K
Absorption coefficient[36]	α	10000 cm^{-1}
Electron saturation velocity[37]	v_{sn}	4×10^4 m/s
Hole saturation velocity[37]	v_{sp}	1×10^4 m/s
Low field electron lifetime[37]	τ_n	0.1 ps
Low field hole lifetime[37]	τ_p	0.4 ps
Low field electron mobility[38]	μ_{n0}	400 cm^2/Vs
Low field hole mobility[38]	μ_{p0}	100 cm^2/Vs
Surface recombination velocity[39]	$s_{n,p}$	5000 m/s

The lengths of the array elements, l_{nm}, and their separation distances in x direction, d'_{nm}, are equal to have a constructive spatial power combination, and can be calculated as

$$\begin{aligned}l_{nm}=&d'_{nm}\\=&\pi\left[\frac{x_{nm}-x_{l1}}{[(x_{nm}-x_{l1})^2+(y_{nm}-y_{l1})^2+z_l^2]^{\frac{1}{2}}}k_1\right.\\&\left.-\frac{x_{nm}-x_{l2}}{[(x_{nm}-x_{l2})^2+(y_{nm}-y_{l2})^2+z_l^2]^{\frac{1}{2}}}k_2\right]^{-1}\end{aligned} \tag{19}$$

where $n=-N,\ldots,N$ and $m=-M,\ldots,-1,1,\ldots,M$.

The thickness of the substrate is determined based on the resonant condition and loss mechanisms of the structure. The best value for the thickness of the substrate for minimum surface mode loss is [35]

$$h=\frac{\pi c}{2\Omega\sqrt{\epsilon_r-1}}. \tag{20}$$

This design procedure guarantees maximum radiation for each of the array elements, but does not necessarily guarantee the maximum radiation for the entire array. To have maximum radiation for the entire array, one has to maximize (14), which is difficult to do analytically. As we will see in the next section, the radiation power from a designed array based on the above mentioned procedure is very close to the maximum radiation of the entire array.

IV. Simulation Results

A 1×31 array configuration is considered for simulation purpose. Since the separation distance of the array elements in y direction is arbitrary, we set it equal to zero to maximize the photo-excited region and increase the radiation power. The array elements are made of low-temperature grown (LTG) GaAs located above a grounded GaAs substrate with the relative permittivity of 12.6. The elements are biased to a dc voltage of 7.5 V. The thickness of the array elements is 2 μm. All the physical parameters for a typical LTG-GaAs material are presented in Table I.

The entire array is excited by two tunable single-mode lasers operating around 780 nm with their frequency difference falling in the terahertz spectrum. The power density from the two lasers is 0.12 $\mathrm{mW}/\mu\mathrm{m}^2$. The LTG-GaAs photomixers can withstand an optical power of 0.9 $\mathrm{mW}/\mu\mathrm{m}^2$ with 4 V/μm dc bias at room

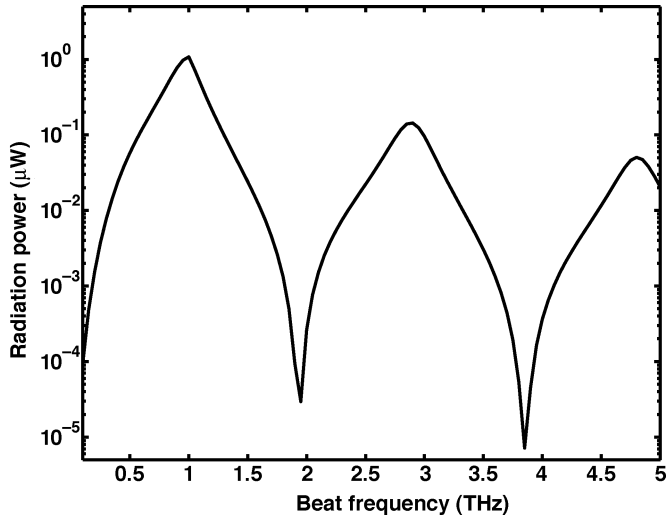

Fig. 3. Total terahertz radiation power versus beat frequency. The thickness of the substrate is fixed for maximum radiation at 1 THz.

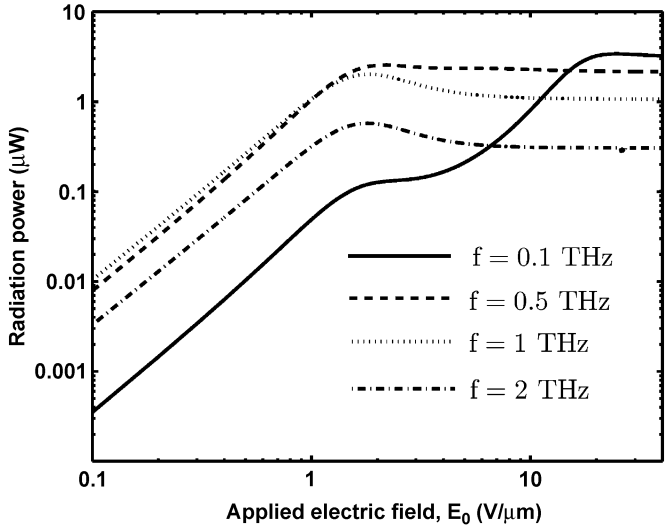

Fig. 4. Total terahertz radiation power versus applied electric field.

temperature [40]. The two lasers are located in $x-z$ plane with $x_{l2}=-x_{l1}=1.3$ mm and $z_l=50$ mm. The array is designed to work at 1 THz. For this frequency, the optimum value for the thickness of the substrate is 21.8 μm. The lengths of the array elements and their separation distances are calculated from (17)–(19), and are around 7.46 μm. The width of the array elements is 120 μm.

Fig. 3 shows the radiation power versus beat frequency for the designed array. The power of each laser is 3.33 W, and the consumed optical power in each element is 107 mW. A Ti:sapphire laser can generate the required optical power. In order to decrease the thermal effects of the absorbed optical power and the applied dc bias, one can use a good thermal conductor layer, such as AlAs layer beneath the LTG-GaAs layer [41]. Operating the photomixer at the low temperatures is another way to increase the maximum sustainable optical power and dc bias of the device [40]. It can be seen from Fig. 3 that around 1 μW power is achievable at 1 THz. The optical-to-electrical efficiency of the device is 0.0032%. The optimum thickness of the substrate is a function of frequency, which makes the structure a narrow band radiator.

Shown in Fig. 4 is the radiated power versus applied dc bias. The applied electric field is the ratio of the applied dc voltage to the length of the array elements. The radiation power saturates with the applied electric field, which is the result of the carrier velocity saturation in the photoconductor. As it can be seen from Fig. 4, for an LTG-GaAs sample with the physical parameters given in Table I, the saturation region starts at the applied electric field around $\mathrm{E}_0=3$ V/μm for the beat frequency above 0.5 THz. The optimum value of the applied dc bias for maximum terahertz radiation and minimum thermal effect is the value corresponding to the starting point of the saturation region.

Fig. 5 shows the radiation power versus beat frequency, where the thickness of the substrate is changed according to the beat frequency to have maximum radiation at each frequency. The applied dc bias is high enough to have the radiation power in its saturation region for all beat frequencies. Note that the

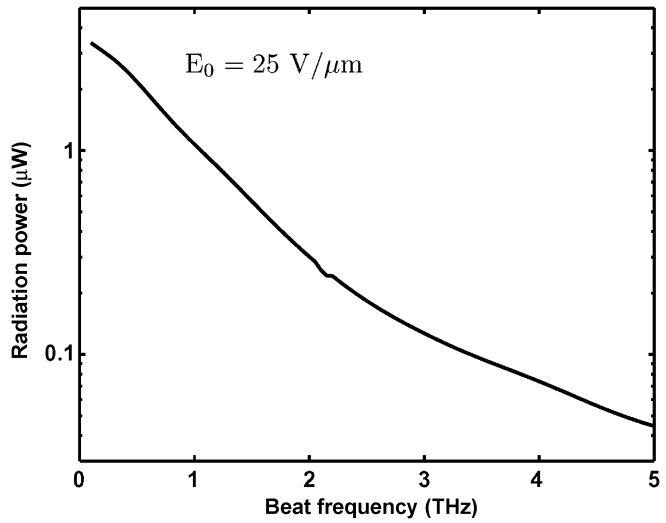

Fig. 5. Total terahertz radiation power versus beat frequency. The thickness of the substrate changes according to the beat frequency to have maximum radiation at each frequency.

applied electric field must be lower than GaAs breakdown field, which is around 40 V/μm [36], [42]. According to Fig. 5, the radiation power decreases with frequency as $1/\Omega$ [29].

From Fig. 1, the angle between the two lasers located in $x-z$ plane can be defined as $\theta_l=\theta_{001}+\theta_{002}=-\tan^{-1}(x_{l1}/z_l)+\tan^{-1}(x_{l2}/z_l)$. Fig. 6 shows the radiation pattern at the plane of $\phi=0$ for different values of θ_l, and for arrays with different number of elements. It can be seen that by changing the angle between the two lasers one can steer the radiation beam. The grating vector $\mathbf{K_{nm}}$ changes by changing the angle between the two lasers, which consequently changes the phase distribution of the current over the array elements and results in pattern deflection. It also can be seen from Fig. 6 that the radiated beam becomes narrower by increasing the number of array elements. Fig. 7 shows the radiation pattern of the designed array at $\phi=0$ and $\phi=\pi/2$ planes. The radiation pattern is symmetric and its side-lobe level is around -13.2 dB.

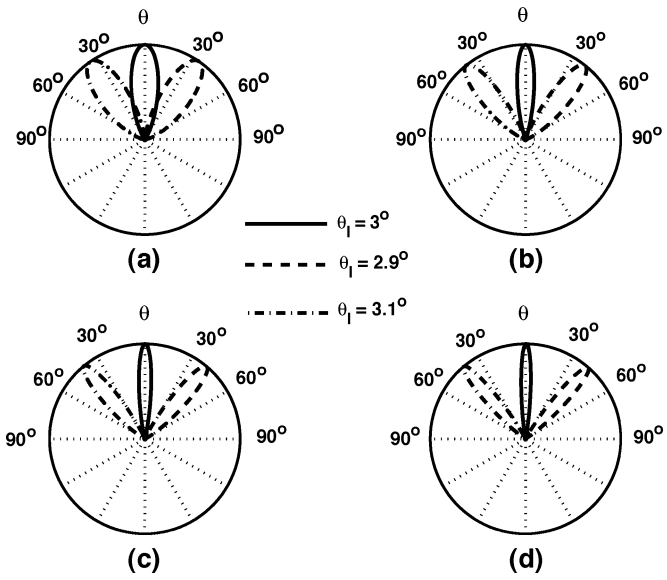

Fig. 6. Radiation pattern at $\phi = 0$ plane for different number of array elements and at the beat frequency of 1 THz; (a) 1×31 array (FWHM $= 6.59°$), (b) 1×51 array (FWHM $= 4°$), (c) 1×71 array (FWHM $= 2.88°$), (d) 1×91 array (FWHM $= 2.3°$).

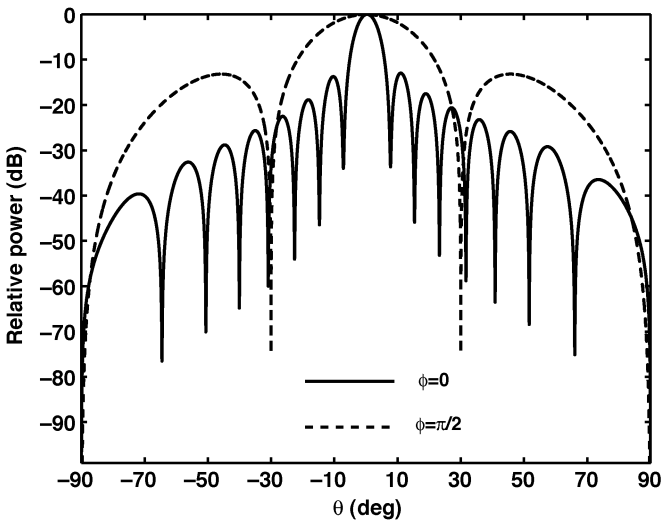

Fig. 7. Radiation pattern at $\phi = 0$ and $\phi = \pi/2$ planes for an 1×31 array at the beat frequency of 1 THz and $\theta_l = 3.02°$.

Shown in Fig. 8 is the radiation power for the different values of the angle between the two lasers. As it can be seen from Fig. 8, the maximum radiation of the entire array occurs at an angle very close to $\theta_l = 3°$. The radiation power rapidly drops for the angles far from the angle that the array is designed for, because at these angles the maximum radiation condition given by (15) is no longer valid. The graph shown in Fig. 8 is asymmetric with respect to θ_l, since the grating vector $\mathbf{K_{nm}}$ is not symmetric with respect to θ_l.

Fig. 9 shows that one can increase the terahertz radiation power by using higher power lasers and increasing the number of array elements. The radiation power does not scale as the square of the number of array elements, while it is proportional to the square of the optical power (see Fig. 10). Hence, for a given optical power the optimum design is an array with minimum number of elements, while each element absorbs its maximum consumable optical power.

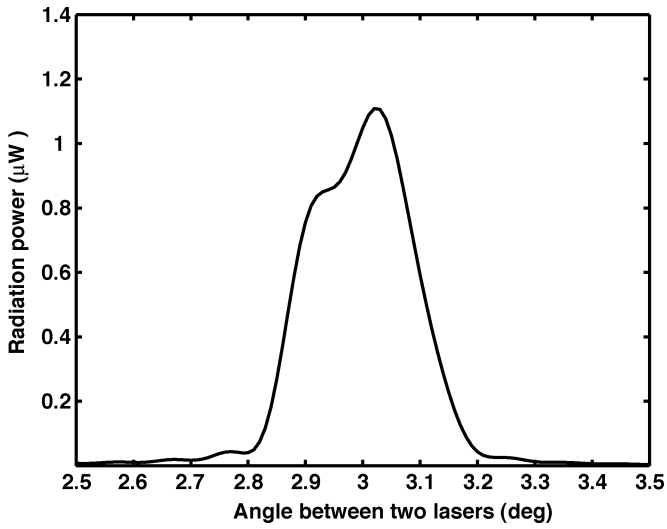

Fig. 8. Radiation power versus angle between two lasers at the beat frequency of 1 THz.

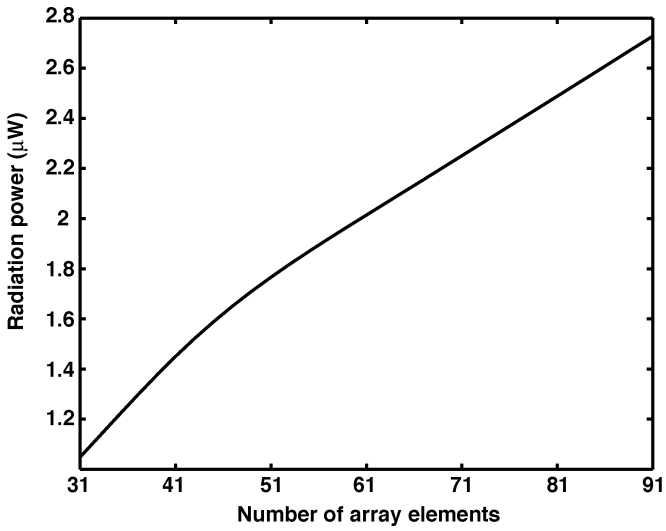

Fig. 9. Radiation power versus number of array elements for a constant optical power density at the beat frequency of 1 THz.

V. Conclusion

A continuous-wave terahertz photomixer array source made of LTG-GaAs has been designed and analyzed. It has been shown that a few μW terahertz power is achievable from a typical array source at 1 THz. The dependency of the radiation power on the beat frequency and the applied dc bias has been studied. It has been shown that the radiated beam can be steered over more than $\pm 30°$ by changing the angle between the two exiting laser beams. The proposed device is suitable for biological and material spectroscopy, medical imaging, and security applications.

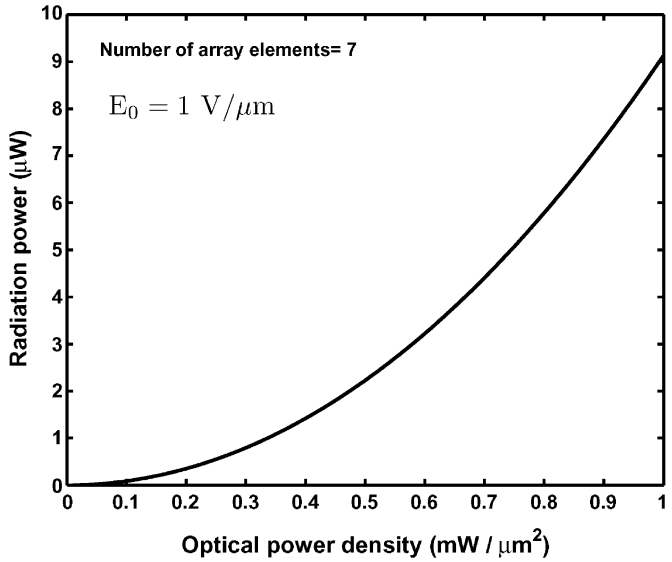

Fig. 10. Radiation power versus optical power density at 1 THz.

APPENDIX I

The photocurrent's components in a typical photoconductive photomixer can be written as [29]

$$J^s_{nm1} = \frac{e}{\alpha^2 + K^2_{nmz}} \times \Big[(\alpha^n_{1nm} v_n - D_n \alpha^n_{2nm} K_{nmx})|\delta\hat{N}_{nm}| + (\alpha^p_{1nm} v_p + D_p \alpha^p_{2nm} K_{xnm})|\delta\hat{P}_{nm}|\Big] \quad (21)$$

$$J^s_{nm2} = \frac{e}{\alpha^2 + K^2_{nmz}} \times \Big[(\alpha^n_{2nm} v_n + D_n \alpha^n_{1nm} K_{nmx})|\delta\hat{N}_{nm}| + (\alpha^p_{2nm} v_p - D_p \alpha^p_{1nm} K_{nmx})|\delta\hat{P}_{nm}|\Big] \quad (22)$$

where $K_{nmz} = k_1 \cos\theta_{nm1} - k_2 \cos\theta_{nm2}$ is the z-component of the grating vector $\mathbf{K_{nm}}$, v_n and v_p are the electron and hole velocities, respectively, D_n and D_p are the electron and hole diffusion coefficients, respectively, and

$$\alpha^{n[p]}_{1nm} = \alpha_{1nm} \cos\phi^{n[p]}_{nm} + \alpha_{2nm} \sin\phi^{n[p]}_{nm} \quad (23)$$

$$\alpha^{n[p]}_{2nm} = \alpha_{2nm} \cos\phi^{n[p]}_{nm} - \alpha_{1nm} \sin\phi^{n[p]}_{nm} \quad (24)$$

$$\alpha_{1nm} = \alpha + e^{-\alpha d}[K_{nmz} \sin(K_{nmz} d) - \alpha \cos(K_{nmz} d)] \quad (25)$$

$$\alpha_{2nm} = K_{nmz}\left[-1 + e^{-\alpha d} \cos(K_{nmz} d)\right] + \alpha e^{-\alpha d} \sin(K_{nmz} d) \quad (26)$$

$$\delta\hat{N}_{nm} = |\delta\hat{N}_{nm}| e^{j\phi^n_{nm}} = \frac{a^n_{nm} + j b^n_{nm}}{a_{nm} + j b_{nm}} \eta_{nm} G_0 \quad (27)$$

$$\delta\hat{P}_{nm} = |\delta\hat{P}_{nm}| e^{j\phi^p_{nm}} = \frac{a^p_{nm} + j b^p_{nm}}{a_{nm} + j b_{nm}} \eta_{nm} G_0 \quad (28)$$

in which

$$a^n_{nm} = \tau_p^{-1} + D_p\left(|\mathbf{K_{nm}}|^2 - \alpha^2\right) + \frac{e}{\epsilon}(\mu_n \bar{N}_{0nm} + \mu_p \bar{P}_{0nm}) \quad (29)$$

$$a^p_{nm} = \tau_n^{-1} + D_n\left(|\mathbf{K_{nm}}|^2 - \alpha^2\right) + \frac{e}{\epsilon}(\mu_n \bar{N}_{0nm} + \mu_p \bar{P}_{0nm}) \quad (30)$$

$$b^n_{nm} = \Omega - v_p K_{nmx} + 2\alpha D_p K_{nmz} \quad (31)$$

$$b^p_{nm} = \Omega + v_n K_{nmx} + 2\alpha D_n K_{nmz} \quad (32)$$

$$a_{nm} = a^n_{nm} a^p_{nm} - b^n_{nm} b^p_{nm} - \frac{e}{\epsilon}\left[\mu_p a^n_{nm} \bar{P}_{0nm} + \mu_n a^p_{nm} \bar{N}_{0nm}\right] \quad (33)$$

$$b_{nm} = a^p_{nm} b^n_{nm} + a^n_{nm} b^p_{nm} - \frac{e}{\epsilon}\left[\mu_p b^n_{nm} \bar{P}_{0nm} + \mu_n b^p_{nm} \bar{N}_{0nm}\right] \quad (34)$$

$$\bar{N}_{0nm} = \frac{1}{\alpha d}(1 - e^{-\alpha d}) N_{0nm} \quad (35)$$

$$\bar{P}_{0nm} = \frac{1}{\alpha d}(1 - e^{-\alpha d}) P_{0nm} \quad (36)$$

$$G_0 = \frac{2\alpha I_0}{[\hbar(\omega_1 + \omega_2)]} \quad (37)$$

where N_{0nm} and P_{0nm} can be calculated from

$$\mu_n \frac{e}{\epsilon} \bar{N}_{0nm}[P_{0nm} - N_{0nm}] + \alpha^2 D_n N_{0nm} - \frac{N_{0nm}}{\tau_n} + G_0 = 0 \quad (38)$$

$$-\mu_p \frac{e}{\epsilon} \bar{P}_{0nm}[P_{0nm} - N_{0nm}] + \alpha^2 D_p P_{0nm} - \frac{P_{0nm}}{\tau_p} + G_0 = 0. \quad (39)$$

REFERENCES

[1] P. H. Siegel, "Terahertz technology in biology and medicine," *IEEE Trans. Microw. Theory Tech.*, vol. 52, no. 10, pp. 2438–2447, Oct. 2004.

[2] T. W. Crowe, T. Globus, D. L. Woolard, and J. L. Hesler, "Terahertz sources and detectors and their application to biological sensing," *Phil. Trans. R. Soc. Lond. A*, vol. 362, no. 1815, pp. 365–377, 2004.

[3] P. H. Bolivar, M. Nagel, F. Richter, M. Brucherseifer, H. Kurz, A. Bosserhoff, and R. Buttner, "Label-free THz sensing of genetic sequences: toward THz biochips," *Phil. Trans. R. Soc. Lond. A*, vol. 362, no. 1815, pp. 323–335, 2004.

[4] T. Globus, D. Woolard, M. Bykhovskaia, B. Gelmont, L. Werbos, and A. Samuels, "THz-frequency spectroscopic sensing of DNA and related biological materials," *Int. J. High Speed Electron. Syst.*, vol. 13, no. 4, pp. 903–936, 2003.

[5] S. Wang, B. Ferguson, D. Abbott, and X. C. Zhang, "T-ray imaging and tomography," *J. Biol. Phys.*, vol. 29, no. 2–3, pp. 247–256, 2003.

[6] B. B. Hu and M. C. Nuss, "Imaging with terahertz waves," *Opt. Lett.*, vol. 20, no. 16, pp. 1716–1718, 1995.

[7] M. Naftaly, A. P. Foulds, R. E. Miles, and A. G. Davies, "Terahertz transmission spectroscopy of nonpolar materials and relationship with composition and properties," *Int. J. Infrared Millimeter Waves*, vol. 26, no. 1, pp. 55–64, 2005.

[8] Y. Watanabe, K. Kawase, T. Ikari, H. Ito, Y. Ishikawa, and H. Minamide, "Component analysis of chemical mixtures using terahertz spectroscopic imaging," *Opt. Commun.*, vol. 234, no. 1–6, pp. 125–129, 2004.

[9] E. R. Brown, J. Bjarnason, T. L. J. Chan, D. C. Driscoll, M. Hanson, and A. C. Gossard, "Room temperature, THz photomixing sweep oscillator and its application to spectroscopic transmission through organic materials," *Rev. Sci. Instrum.*, vol. 75, no. 12, pp. 5333–5342, 2004.

[10] T. L. J. Chan, J. E. Bjarnason, A. W. M. Lee, M. A. Celis, and E. R. Brown, "Attenuation contrast between biomolecular and inorganic materials at terahertz frequencies," *Appl. Phys. Lett.*, vol. 85, no. 13, pp. 2523–2525, 2004.

[11] D. Mittleman, Ed., *Sensing With Terahertz Radiation*. Germany: Springer-Verlag, 2003.

[12] N. Karpowicz, H. Zhong, C. Zhang, K.-I. Lin, J.-S. Hwang, J. Xu, and X.-C. Zhang, "Compact continuous-wave subterahertz system for inspection applications," *Appl. Phys. Lett.*, vol. 86, no. 5, p. 54 105-3, 2005.

[13] M. K. Choi, A. Bettermann, and D. W. Van Der Weide, "Potential for detection of explosive and biological hazards with electronic terahertz systems," *Phil. Trans. R. Soc. Lond. A*, vol. 362, no. 1815, pp. 337–349, 2004.

[14] M. C. Kemp, P. F. Taday, B. E. Cole, J. A. Cluff, A. J. Fitzgerald, and W. R. Tribe, "Security applications of terahertz technology," in *Proc. SPIE Conf.*, vol. 5070, Aug. 2003, pp. 44–52.

[15] D. Woolard, R. Kaul, R. Suenram, A. Hight Walker, T. Globus, and A. Samuels, "Terahertz electronics for chemical and biological warfare agent detection," in *IEEE MTT-S Int. Microwave Symp. Dig.*, 1999, pp. 925–928.
[16] P. F. Taday, "Applications of terahertz spectroscopy to pharmaceutical sciences," *Phil. Trans. R. Soc. Lond. A*, vol. 362, no. 1815, pp. 351–364, 2004.
[17] V. P. Wallace, P. F. Taday, A. J. Fitzgerald, R. M. Woodward, J. Cluff, R. J. Pye, and D. D. Arnone, "Terahertz pulsed imaging and spectroscopy for biomedical and pharmaceutical applications," *Faraday Discuss.*, vol. 126, pp. 255–263, 2004.
[18] T. Nagatsuma, "Millimeter-wave photonic technologies for communications and sensor applications," in *New Photonics Technologies for the Information Age: The Dream of Ubiquitous Services*, S. Sudo and K. Okamoto, Eds. Norwood, MA: Artech House, 2004, pp. 193–212.
[19] C. M. Mann, "Toward terahertz communications systems," in *Terahertz Sources and Systems*, R. E. Miles, P. Harrison, and D. Lippens, Eds. Norwell, MA: Kluwer, 2001, pp. 261–267.
[20] A. Hirata, H. Ishii, and T. Nagatsuma, "Design and characterization of a 120-GHz millimeter-wave antenna for integrated photonic transmitters," in *Proc. Int. Topical Meeting on Microwave/Photonics*, 2000, pp. 229–232.
[21] M. C. Teich, "Field-theoretical treatment of photomixing," *Appl. Phys. Lett.*, vol. 14, no. 6, pp. 201–203, 1969.
[22] J. Soohoo, S.-K. Yao, J. E. Miller, R. R. Shurtz, Y. Taur, and R. A. Gudmundsen, "A laser-induced traveling-wave device for generating millimeter waves," *IEEE Trans. Microw. Theory Tech.*, vol. MTT-29, no. 11, pp. 1174–1181, Nov. 1981.
[23] G. J. Simonis and K. G. Purchase, "Optical generation, distribution and control of microwaves using laser heterodyne," *IEEE Trans. Microw. Theory Tech.*, vol. 38, no. 5, pp. 667–669, May 1990.
[24] E. R. Brown, F. W. Smith, and K. A. McIntosh, "Coherent millimeter-wave generation by heterodyne conversion in low-temperature-grown GaAs photoconductors," *J. Appl. Phys.*, vol. 73, no. 3, pp. 1480–1484, 1993.
[25] S. Matsuura, G. A. Blake, R. A. Wyss, J. C. Pearson, C. Kadow, A. W. Jackson, and A. C. Gossard, "A traveling-wave THz photomixer based on angle-tuned phase matching," *Appl. Phys. Lett.*, vol. 74, no. 19, pp. 2872–2874, 1999.
[26] C. J. Stevens and D. J. Edwards, "Photomixing receiver using the kinetic inductive effect in high T_c superconductors," *Electron. Lett.*, vol. 37, no. 23, pp. 1420–1421, 2001.
[27] E. R. Brown, "THz generation by photomixing in utlrafast photoconductors," *Int. J. High Speed Electron. Syst.*, vol. 13, no. 2, pp. 497–545, 2003.
[28] M. Naftaly, M. R. Stone, A. Malcoci, R. E. Miles, and I. C. Mayorga, "Generation of CW terahertz radiation using two-color laser with Fabry-Perot etalon," *Electron. Lett.*, vol. 41, no. 3, pp. 128–129, 2005.
[29] D. Saeedkia, R. R. Mansour, and S. Safavi-Naeini, "The interaction of laser and photoconductor in a continuous-wave terahertz photomixer," *IEEE J. Quantum Elect.*, vol. 41, no. 9, pp. 1188–1196, September 2005.
[30] ——, "Modeling and analysis of high-temperature superconductor terahertz photomixers," *IEEE Trans. Appl. Superconduct.*, vol. 15, no. 3, September 2005.
[31] D. Saeedkia, A. H. Majedi, S. Safavi-Naeini, and R. R. Mansour, "Analysis and design of a photoconductive integrated photomixer/antenna for terahertz applications," *IEEE J. Quantum Elect.*, vol. 41, no. 2, pp. 234–241, 2005.
[32] ——, "High-temperature superconductive photomixer patch antenna: theory and design," *IEICE Trans. Elecron.*, vol. E86-C, no. 7, pp. 1318–1327, Jul. 2003.
[33] D. R. Jackson and J. T. Williams, "A comparison of CAD models for radiation from rectangular microstrip patches," *Int. J. Microw. Millimeter-Wave Comp. Aided Eng.*, vol. 1, no. 2, pp. 236–248, 1991.
[34] C. A. Balanis, *Antenna Theory: Analysis and Design*. New York: Wiley, 1997.
[35] ——, *Advanced Engineering Electromagnetics*. New York: Wiley, 1989, ch. 8.
[36] S. M. Sze, *Physics of Semiconductor Devices*. New York: Wiley, 1981, pp. 50–51.
[37] E. R. Brown, "A photoconductive model for superior GaAs THz photomixer," *Appl. Phys. Lett.*, vol. 75, no. 6, pp. 769–771, 1999.
[38] E. R. Brown, K. A. McIntosh, F. W. Smith, K. B. Nichols, M. J. Manfra, C. L. Dennis, and J. P. Mattia, "Milliwatt output levels and superquadratic bias dependence in a low-temperature-grown GaAs photomixer," *Appl. Phys. Lett.*, vol. 64, no. 24, pp. 3311–3313, 1994.
[39] D. E. Aspnes, "Recombination at semiconductor surfaces and inter-fates," *Surface Sci.*, vol. 132, pp. 406–421, 1983.
[40] S. Verghese, K. A. McIntosh, and E. R. Brown, "Optical and terahertz power limits in the low-temperature-grown GaAs photomixers," *Appl. Phys. Lett.*, vol. 71, no. 19, pp. 2743–2745, 1997.
[41] A. W. Jackson, "Low-temperature-grown GaAs photomixers designed for increased terahertz output power," Ph.D. dissertation, Univ. California Santa Barbara, 1999.
[42] R. A. Smith, *Semiconductors*, 2nd ed. Cambridge, U.K.: Cambridge Univ. Press, 1978.

Daryoosh Saeedkia (S'04–M'05) was born in Tehran, Iran, on October 7, 1971. He received the B.Sc. and M.Sc. degrees in electrical engineering from Sharif University of Technology, Tehran, in 1995 and 2001, respectively, and the Ph.D. degree in electrical and computer engineering from the University of Waterloo, Waterloo, ON, Canada, in 2005.

From 1995 to 2001, he was with the Optical Fiber and Solar Cell Fabrication Co. (OFSCFC), Tehran, as Head Engineer of the optical fiber production line. He is currently a Postdoctoral Fellow in the RF/Microwave and Photonics Research Group at the University of Waterloo. His research interests include generation and detection of terahertz signals using photoconductor and superconductor photomixers, terahertz technology, and microwave photonics devices.

Raffat R. Mansour (S'84–M'86–SM'90–F'01) was born in Cairo, Egypt, on March 31, 1955. He received the B.Sc. (with honors) and M.Sc. degrees from Ain Shams University, Cairo, in 1977 and 1981, respectively, and the Ph.D. degree from the University of Waterloo, ON, Canada, in 1986, all in electrical engineering.

He was a Research Fellow at the Laboratoire d'Electromagnetisme, Institut National Polytechnique, Grenoble, France, in 1981. From 1983 to 1986, he was a Research and Teaching Assistant with the Department of Electrical Engineering, University of Waterloo. He joined COM DEV Ltd. Cambridge, ON, Canada, in 1986, where he held several technical and management positions in the Corporate Research and Development Department. He was promoted to Scientist in 1998. In January 2000, he joined the University of Waterloo as Professor in the Electrical and Computer Engineering Department. He holds a Research Chair at the University of Waterloo in RF Technologies. He holds several patents related to microwave filter design for satellite applications, and he has numerous publications in the area of electromagnetic modeling and high temperature superconductivity. His present research interests include Superconductive technology, MEMS technology and CAD design of RF circuits for wireless and satellite applications.

Safieddin Safavi-Naeini (S'75–M'78) was born in Gachsaran, Iran, in 1951. He received the B.Sc. degree in electrical engineering, from the University of Tehran, Tehran, Iran, in 1974 and the MSc. and Ph.D. degrees in electrical engineering, from the University of Illinois at Urbana-Champaign, USA, in 1975 and 1979, respectively.

He joined the Electrical Engineering Department, University of Tehran, as an Assistant Professor in 1980 and became an Associate Professor in 1988. He joined the University of Waterloo, Waterloo, ON, Canada, in 1996, where he is currently a full Professor in the Electrical and Computer Engineering Department. He holds an NSERC/RIM Industrial Research Chair at the University of Waterloo in Intelligent Integrated Radio and Photonics. His research interests and activities include numerical electromagnetics applied to RF/microwave/millimeter wave systems and circuits, antenna and propagation, wireless communication systems, very high speed digital circuits, and optical communication systems. He has been scientific and technical consultant to a number of national and international telecommunication industrial and research organizations since 1980.